Parallel collective resonances in arrays of gold nanorods

Alan Vitrey†, Lionel Aigouy‡, Patricia Prieto†, José Miguel García-Martín†, María U. González*†*

†Instituto de Microelectrónica de Madrid (IMM), Isaac Newton 8, 28760 Tres Cantos, Madrid, Spain

‡Laboratoire de Physique et d'Etude des Matériaux (LPEM), UMR CNRS 8213, Ecole Supérieure de Physique et de Chimie Industrielles (E.S.P.C.I.), 10 Rue Vauquelin, 75231 Paris Cedex 05, France

ABSTRACT. In this work we discuss the excitation of parallel collective resonances in arrays of gold nanoparticles. Parallel collective resonances result from the coupling of the nanoparticles localized surface plasmons with diffraction orders travelling in the direction parallel to the polarization vector. While they provide field enhancement and delocalization as the standard collective resonances, our results suggest that parallel resonances could exhibit greater tolerance to index asymmetry in the environment surrounding the arrays. The near- and far-field properties of these resonances are analyzed, both experimental and numerically.

KEYWORDS. Surface plasmons, nanoparticles, collective resonances, near-field optical microscopy (SNOM), near-field patterns, Rayleigh anomalies.

Metallic nanoparticles exhibit remarkable optical properties associated with the excitation of localized surface plasmon resonances (LSPRs), which enable an ever increasing number of applications related to enhanced and more confined light-matter interaction, control of emission and sensing.[1] Furthermore, these properties can be modified and promoted by adjusting the interaction between nanoparticles. So, near-field interactions between very close nanoparticles shift the resonance position anisotropically,[2] induce an even stronger field enhancement between the nanoparticles,[3] and improve sensing capabilities.[4] Complex nanoclusters can generate collective modes of different nature, which provide a further control of the spectral response through Fano resonances.[5,6] In recent years, interactions between nanostructures in arrays mediated by diffraction orders have also received an increasing amount of attention.[7–20] At wavelengths close to a Rayleigh anomaly (RA), which corresponds to the transition from an evanescent to a propagative diffraction order in an array, the nanoparticles LSPRs can couple with these diffracted waves and give rise to the so called collective, lattice or geometric resonances.[14,15]

Collective resonances induce several differences between the extinction spectrum of an array and that of an isolated nanostructure, such as a shift of the main extinction peak, the presence of a dip, and, more interestingly, the appearance of a supplementary extinction peak with an asymmetric shape and a potential high quality factor.[9,12,15] Moreover, the collective resonance is concomitant with an increase of the plasmonic enhancement of the near-field, as well as its delocalization.[18,21–23] These far- and near-field properties make geometric resonances of great interest for several applications such as sensing,[24–27] enhanced surface Raman scattering (SERS),[28] or enhancement and control of spontaneous[29–34] and stimulated[35] emission.

So far, the canonical excitation of collective resonances is achieved at normal incidence and with the polarization vector of the incident electric field set orthogonally to the plane of the diffraction wavevector participating in the mode. In the particular case of 1D arrays –chains–, the light polarization has to be perpendicular to the chain axis.[9] This is understood by taking into account the key element leading to the excitation of collective resonances: the contribution of all the nanoparticles, considered as dipoles, to the total field seen locally by each one of them.[9,14,15] In a homogeneous medium, this contribution is dominated by the far-field component of the dipolar emission, which emerges in the plane perpendicular to the dipole orientation. From now on, we will denote this as the orthogonal collective resonance. The experimental validation of lattice resonances has mainly dealt with this orthogonal configuration and has stressed the importance of the presence of the homogeneous medium to excite the geometrical modes.[12,15] Additionally, theoretical works have pointed out the fact that the far-field contribution diminishes considerably due to multiple interferences induced by the presence of a substrate, hence decreasing the strength of the collective resonance until it vanishes.[36] Therefore, nanoparticle arrays embedded in an inhomogeneous medium, such as an interface, are not likely to support this orthogonal collective resonances unless the system matches two conditions: i) the particles are big enough to show a significant scattering cross-section, and ii) the difference in refraction index between the upper and lower medium is limited.[22,36,37] These requirements could in some cases hinder the application of collective resonances.

In this letter we demonstrate, both experimental and numerically, that metallic nanostructures at a glass/air interface are able to support collective resonances when using the parallel configuration, *i.e.* when the incident polarization vector is parallel to the diffraction vector participating in the mode. On the other hand, no contribution from orthogonal coupling has been

detected, probably because of the high index asymmetry. The studied 2D arrays consist of gold nanorods where LSPRs are excited along the rods' short axis. These arrays show in their extinction spectra the presence of a narrow peak in the vicinity of the RA associated with diffraction along this short axis, which signals the excitation of a parallel lattice resonance. The near-field properties of these resonances, assessed by scanning near-field optical microscopy (SNOM) and supported by finite difference time domain (FDTD) modeling, also account for an enhancement of the near-field values and a delocalization of the field. These modes can therefore be exploited in the same application niches as the orthogonal collective resonances, with the advantage of a higher robustness to refractive index mismatch.

The analyzed nanorod arrays have been fabricated by e-beam lithography and dry etching on BK7 glass substrate (see details in the Supporting Information). Figure 1a shows one of the fabricated arrays imaged by SEM. In this study, the nanorods are always illuminated with light polarized along their short axis, so we will denote the array periodicity along that direction as $T_{\parallel}$ and the array periodicity along the rods length as $T_{\perp}$. The nanorods' width is named w. The selection of the appropriate values for the different geometric parameters of the arrays has followed the strategy sketched in Figure 1b, which is exposed in the ensuing paragraph.

The spectral position of the nanorods LSPR along the in-plane short axis (transverse LSPR) is determined by the aspect ratio of the rods' lateral dimensions. To limit disparities in the plasmonic behavior between arrays, we have kept the rods' length and height constant, and then the transverse LSPR position is controlled by w. The excitation of collective resonances is associated with coupling between the nanostructures through the diffracted order propagating along the array plane, which corresponds to the RA and whose wavelength for each array periodicity is given by $RA^{\alpha}_{\parallel,\perp} = n^{\alpha} T_{\parallel,\perp}$, with n^{α} the refractive index of the medium in which the

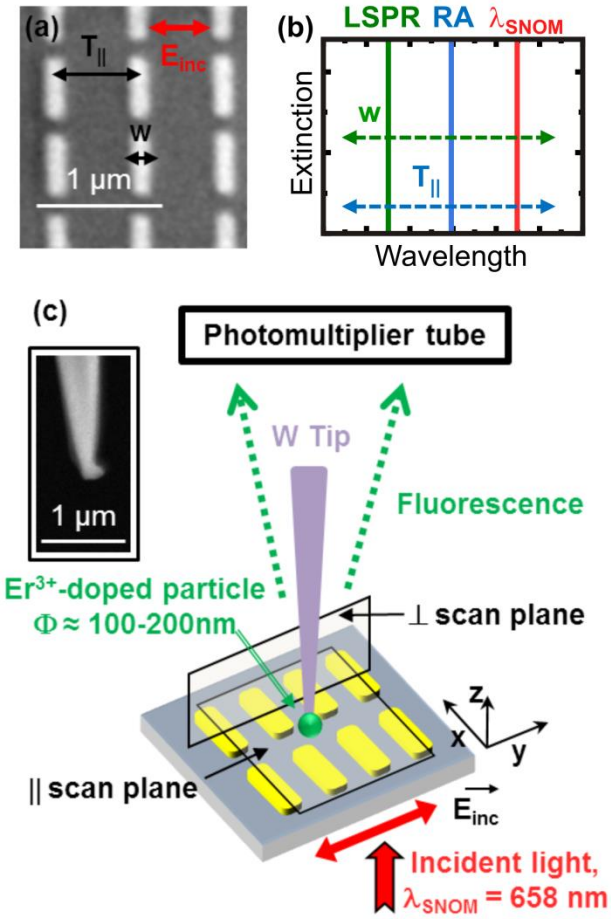

Figure 1. (a) SEM picture of a representative array of gold nanorods. $T_{||}$ and w are the array period along the axis parallel to the incident polarization and the width of the nanorods, respectively. (b) Scheme of the approach used to modify the degree of LSPR-$RA_{||}$ coupling and its position with respect to the wavelength of the SNOM laser, λ_{SNOM} (red line). By varying $T_{||}$ from an array to another, the Rayleigh anomaly $RA_{||}$ (blue line) is shifted closer or farther to λ_{SNOM}. Modifications on w shift the wavelength of the LSPR (green line), which allows obtaining different LSPR–$RA_{||}$ coupling regimes determined by the $RA_{||}$ and LSPR relative positions. (c) Scheme of principle of the SNOM measurements. The arrays are illuminated from below at normal incidence with a laser beam (λ_{SNOM} = 658 nm). The incident light is polarized along the rods short axis. A fluorescent nanoparticle attached to a tip is scanned over the sample and gets excited by the near-field, emitting light at a different wavelength that is collected by a photomultiplier tube. Both scans parallel (within the *xy* plane) and perpendicular (containing the *z* axis) to the surface plane can be performed. The inset shows a SEM picture of the tip with a fluorescent nanoparticle glued at its extremity.

order of diffraction becomes propagative (air or BK7 in our case). The use of this formula is valid all along this work since we only consider the excitation of the first order of diffraction

under normal incidence. In order to characterize the different coupling regimes between the nanorods LSPR and the parallel diffraction orders, we have modified their relative positions from array to array by changing the values of w and/or $T_{||}$, respectively. Moreover, to allow the near-field characterization of this coupling, we need to position the transverse LSPR and $RA_{||}$ accordingly to the value of the wavelength of the laser used in the SNOM experiments, λ_{SNOM} = 658 nm (see Figure 1c). Indeed, as the SNOM measurements allow us to recover the field distribution in the air interface, we only consider $RA_{||}^{air}$. Finally, the value of $T_{\perp}$ is chosen to avoid any potential coupling with the orthogonal diffraction order near λ_{SNOM}. With all these constraints, the geometrical parameters of the arrays are: rods' height, 60 ± 1 nm; length, ~480 nm; w ranging from 120 to 150 nm (lateral uncertainties ± 12 nm); $T_{\perp}$ = 610 nm; and $T_{||}$ varied from 400 to 660 nm.

Figure 2 shows the normalized extinction cross section σ_{Norm}, defined as the extinction cross-section per unitary cell normalized to the nanorods area, of four representative arrays when illuminated from the substrate at normal incidence with a collimated light beam. Both experimental data and FDTD numerical simulations are shown in the graphs (black and purple lines, respectively). The numerical spectra show a good agreement with the experimental ones, reproducing the main features and the overall lineshape even though the calculations consider infinite arrays and the array areas are around 50×50 μm^2. The differences in magnitude between calculated and experimental spectra, not so relevant for the purpose of this study, can be mainly attributed to disparities between the modeled nanorod geometry and the actual one. The details on far-field characterization and FDTD calculations can be found in the Supporting Information.

The spectra in Figure 2a correspond to an array of w = 130 nm, $T_{||}$ = 400 nm. The main feature of the spectrum is the LSPR peak, centered around 640 nm, which is slightly shifted from the

expected position for an isolated nanorod of the same dimensions (around 660 nm), an effect that can be already attributed to collective interactions between the nanorods.[12] Moreover, both in the experimental and numerical spectra, the peak symmetry is slightly affected by a sharp change in the curvature at its left side. We attribute this effect to the appearance of the first order of diffraction towards the substrate associated with $T_{||}$, $RA_{||}^{BK7} = 606$ nm. We have ruled out the possibility that this change is due to the orthogonal configuration, $RA_{\perp}^{air} = 610$ nm, since we have obtained the same effect for an array with $T_{\perp}$ = 310 nm (see Supporting Information). This alteration in the peak shape at the short wavelengths tail has already been reported in the case of the orthogonal configuration and was interpreted as a weakened version of the collective resonances.[15] The weakening is due to low radiative coupling between nanoparticles as the diffraction orders take place at higher energies than the LSPR. Regarding $RA_{||}^{air}$, its value is 400 nm here, which is out of the LSPR peak, so that from now on we will refer to this array as the "Uncoupled" one.

By bringing $RA_{||}^{air}$ towards the long wavelength tail of the rods LSPR peak, diffraction and LSPR can now start to couple. Figure 2b corresponds to an array with w = 120 nm and $T_{||}$ = 648 nm. In this case, a small sharp peak appears close to $RA_{||}^{air}$ in the numerical spectrum while the measurements show only a small asymmetry in the peak shape. The lack of the sharp peak in the experimental data can be attributed to inhomogeneity in the fabricated rods, the finite size of the array,[38,39] and a higher divergence in the illumination and detection as compared with the numerical calculations. The sharp peak indicates the excitation of a collective mode associated to $RA_{||}^{air}$ in this array, although its small amplitude shows that only a weak coupling is obtained as

$RA_{\parallel}^{air}$ is shifted with respect to the LSPR position. From now on we will denote this array as "Weakly coupled".

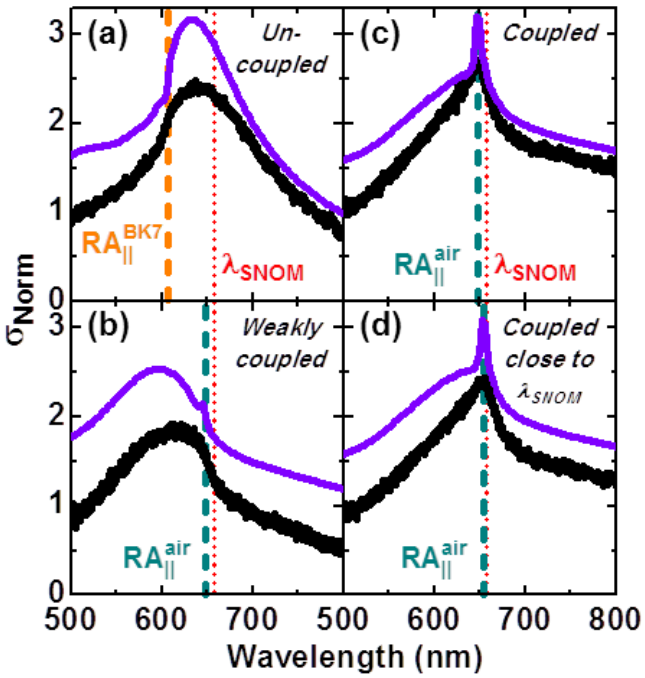

Figure 2. Experimental (black) and simulated (purple) normalized extinction cross section spectra of four Au nanorods arrays: (a) "Uncoupled", with w = 130 nm, $T_{\parallel}$ = 400 nm (LSPR and $RA_{\parallel}^{air}$ are here uncoupled); (b) "Weakly coupled", with w = 120 nm, $T_{\parallel}$ = 648 nm (LSPR and $RA_{\parallel}^{air}$ start here to overlap); (c) "Coupled", with w = 150 nm, $T_{\parallel}$ = 648 nm (LSPR and $RA_{\parallel}^{air}$ overlap, but out of the SNOM wavelength, λ_{SNOM}); (d) "Coupled close to λ_{SNOM}", with w = 150 nm, $T_{\parallel}$ = 654 nm (LSPR, $RA_{\parallel}^{air}$ and λ_{SNOM} overlap). The red dotted line points out the position of λ_{SNOM}. The dashed lines represent the Rayleigh Anomalies position, $RA_{\parallel}$, associated with $T_{\parallel}$ in air or in BK7, depending on the relevant value for each array. In all arrays, $T_{\perp}$ = 610 nm.

Figure 2(c) shows σ_{Norm} for an array with w = 150 nm and $T_{\parallel}$ = 648 nm. Compared to the array in Figure 2(b), here the LSPR position is shifted to longer wavelengths as the nanorods are wider, leading to an improved overlap with $RA_{\parallel}^{air}$. As a consequence, we observe a much better defined sharp peak in the calculated spectrum and a pointed peak in the experimental one. This array is then named "Coupled", but as indicated in the graph the position of $RA_{\parallel}^{air}$ does not

coincide here with λ_{SNOM} (vertical red dotted line in the figure). Figure 2(d) corresponds to an array with w = 150 nm and $T_{||}$ = 654 nm, very close to the value of λ_{SNOM}. Here, LSPR and $RA_{||}^{air}$ still overlap as LSPR is quite broad, and again a sharp peak is present in the spectrum, very similar to that of Figure 2(c). Due to the close position of the collective resonance with λ_{SNOM} in this case, this array is then denoted "Coupled close to λ_{SNOM}".

In summary, in clear contrast to previous works found in the literature,[9,14,15] these spectra suggest the excitation of a collective mode: i) in the presence of a strong mismatch in refractive index between the substrate and the superstrate; and ii) in the parallel configuration. Indeed, no signatures of coupling along the orthogonal direction appear, probably due to the strong index mismatch. The extinction spectra show that these collective modes in the parallel configuration take place very close to $RA_{||}$ position, and that they also give rise to sharp narrow peaks. To get a deeper insight on the properties of these lattice modes, and how the coupling occurs, we have analyzed the near-field distribution of the same four representative arrays.

Near-field analysis has been carried out by SNOM, using a configuration that allows scanning both parallel and perpendicular to the surface plane (see Figure 1c). A SNOM technique based on the use of a fluorescent nanoparticle has been employed (see more details in the Supporting Information), which has been recently demonstrated to provide near-field images in good agreement with numerical simulations.[40,41] The experimental near-field data are correlated with numerical field maps obtained, as for the far-field spectra, by FDTD computations considering infinite arrays of nanorods. Although the nanoparticle fluorescence has been measured to be slightly non-linear with the excitation power (λ_{SNOM} = 658 nm), a good agreement between the calculations and the experimental results is found by taking the intensity of the total electromagnetic field, E_{tot}^2. The horizontal scans are simulated by taking the field distribution at

a height of 170 nm over the substrate, and all the images are convoluted with a circular mask of 150 nm to emulate the nanoparticle diameter (more details in the Supporting Information). Figures 3 and 4 present the distributions of the near-field in the horizontal and vertical planes, respectively, for the same four arrays considered in Figure 2. Figures 3a-d and 4a-d correspond to the SNOM results, and Figures 3e-h and 4e-h to the FDTD calculations.

The near-field distribution of the "uncoupled" array mainly corresponds to that of LSPR excitation, as λ_{SNOM} is close to the LSPR maximum, as shown in Figure 2a. In this case, the maximum value of detected intensity is around 0.4. In all the other arrays, where the parallel lattice mode is excited, we observe an increase of the detected signal of almost one order of magnitude: the maximum value of detected intensity ranges from 3.0 to 3.8 in the case of the horizontal scans and from 2 to 3 for the vertical ones. The "coupled" array shows more intensity than the "weakly coupled" one, and a slight increase in intensity is still experimented when the collective resonance is closer to λ_{SNOM}. These images demonstrate that LSPR-$RA_{||}$ coupling gives rise to a strong field enhancement, of almost one order of magnitude, an effect similar to that found in the orthogonal configuration.[18,21–23]

Regarding the near-field patterns, localized spots are seen in the SNOM maps of the "uncoupled" array, in agreement with the assignation of this distribution to the LSPR.[41] The pattern evolves towards a more delocalized one for the three "coupled" arrays. In the case of "weakly coupled", the in-plane distribution presents columns of bright spots along fainter bands running parallel to the nanorods long axis. This linear pattern becomes more evident and intense for the "coupled" and "coupled close to λ_{SNOM}" arrays. In the three cases, the vertical scan presents a similar chessboard-like pattern, just differing in the degree of vertical delocalization. The field becomes more delocalized, *i.e.* it is enhanced at a higher altitude, as the degree of

coupling increases. Only a faint increase in delocalization, however, is observed from the "coupled" array to the "coupled close to λ_{SNOM}" one.

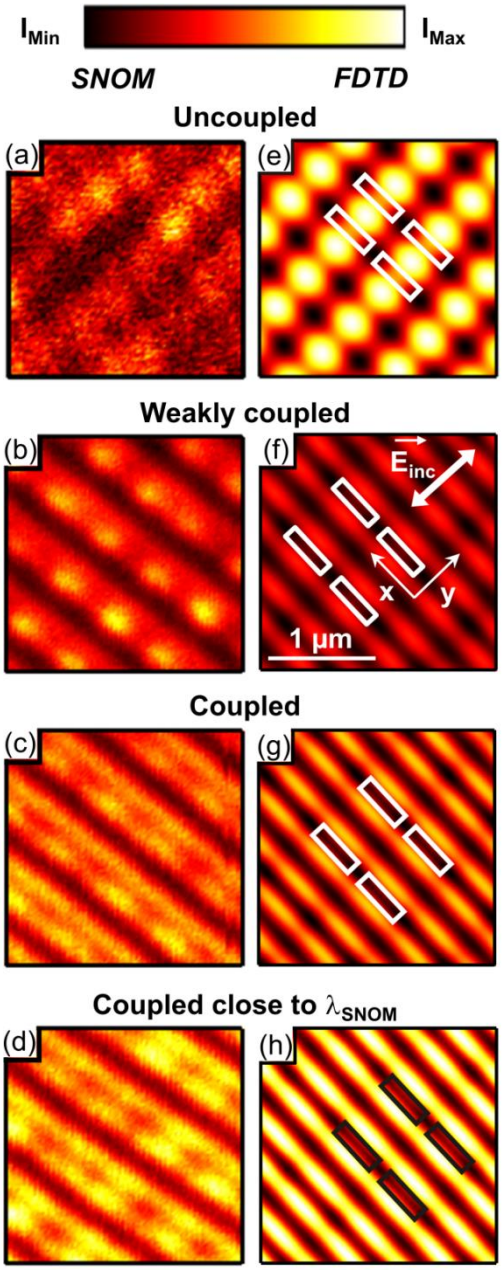

Figure 3. (a)-(d) SNOM images obtained from horizontal scans and (e)-(h) corresponding numerical field maps for the four considered arrays. The lateral size of both scanned and simulated areas is 2.2 µm. The top color bar indicates the normalized level of detected signal in the experiments, I, and the value of the total electric field intensity in the simulations, E_{tot}^2. I_{min} and I_{max} correspond, respectively, to: (a) 0 and 0.4; (b)-(d) 0 and 3.8; (e) 0.2 and 0.6; (f)-(h) 1.1 and 4.4. In (e)-(g), the white rectangles (black ones for (h)) indicate the nanorods positions.

The simulations reproduce well the main elements observed in the experimental near-field patterns. The comparison of the computed near–fields help to pinpoint the differences between the patterns of the three coupled arrays: the same elements are actually present in all the distributions, but differing in their relative intensities. Indeed, for the horizontal scan the spots are slightly more apparent than the lines in the case of the "weakly coupled" array, while the lines strongly dominate for the "coupled close to λ_{SNOM}" one. For the cross-sections, the chess board-like pattern is present with the same intensity in all three cases, but as the degree of

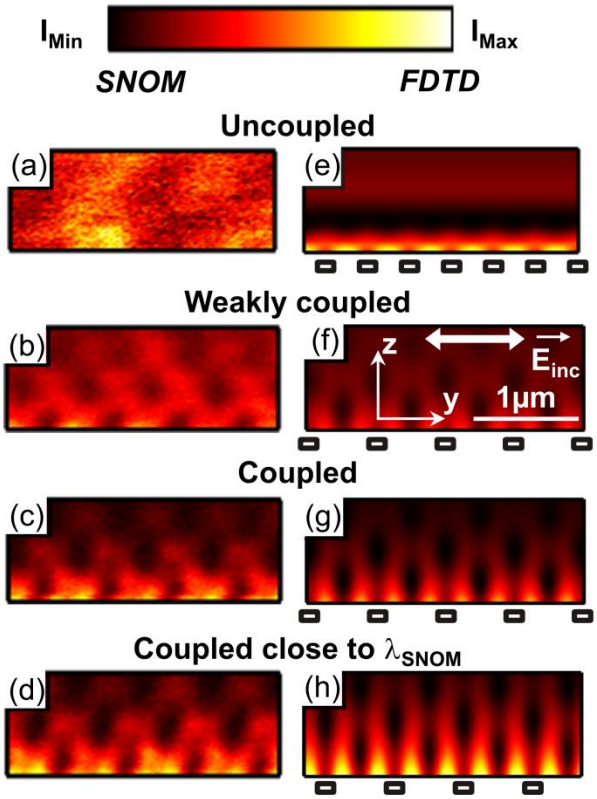

Figure 4. (a)-(d) SNOM images obtained from vertical scans and (e)-(h) numerical field maps for the four considered arrays. Scanned and simulated areas are about 2.6 µm width and 1 µm height. The top color bar indicates the normalized level of detected signal in the experiments, I, and the value of the total electric field intensity, E^2_{tot}, in the simulations. I_{min} and I_{max} correspond, respectively, to: (a) 0 and 0.4; (b)-(d) 0 and 3.0; (e) 0.3 and 0.6; (f)-(h) 0.7 and 4.4. Black rectangles below the field maps in (e)-(h) indicate the nanorods positions.

coupling and matching with λ_{SNOM} increases, vertical rising tails start to dominate the pattern. This pattern is different from the one that has been calculated for the orthogonal collective resonances,[23,29] where the field is more strongly delocalized in the plane than in the vertical direction, and the field enhancement takes place between the nanoparticles along the axis perpendicular to the periodicity responsible of the lattice mode.

To get more understanding on the overall pattern formation, we have analyzed the contributions of the two non null components of the electric field, the in-plane component parallel to the incident polarization $E_{||}$ and the component normal to the array plane E_z. Figure 5 presents $E_{||}$ and E_z for the "weakly coupled" and the "coupled" arrays. Both the planar-view distribution and the vertical cross-section are shown. These simulations show that $E_{||}$ is responsible of the spots in the horizontal scans and the chessboard patterns in the vertical ones, while E_z gives rise to the in-plane linear elements and the vertical rising tails. Regarding the intensity values, $E_{||}$ does not undergo notable variations while the E_z doubles its value for the "coupled" array. This is again in clear contrast with the orthogonal configuration, where no increase and delocalization of E_z takes place and $E_{||}$ is the enhanced component of the field.[23] In fact, the excitation of diffracted orders in the parallel configuration is expected to have strong E_z component. For wavelengths longer than $RA_{||}$, as it is the case here, two counter-propagating evanescent waves travelling along the *y* axis are excited through $T_{||}$. Their E_z component will give rise to an interference pattern along the $T_{||}$ axis with periodicity $T_{||}/2$, as observed in Figure 5. A smaller $E_{||}$ component, mixed to the LSP contribution, will also be present in these waves. The interference between the incident light –polarized along $T_{||}$– and the $E_{||}$ contribution of the two counterpropagative evanescent waves gives rise to the chessboard-like pattern observed in the $E_{||}$ vertical cross-sections of Figure 5 (see details in the Supplementary

Information). As the coupling between LSPR and $RA_{||}$ increases, the contribution of E_z becomes more important and that of $E_{||}$ represents a smallest portion of the total signal.

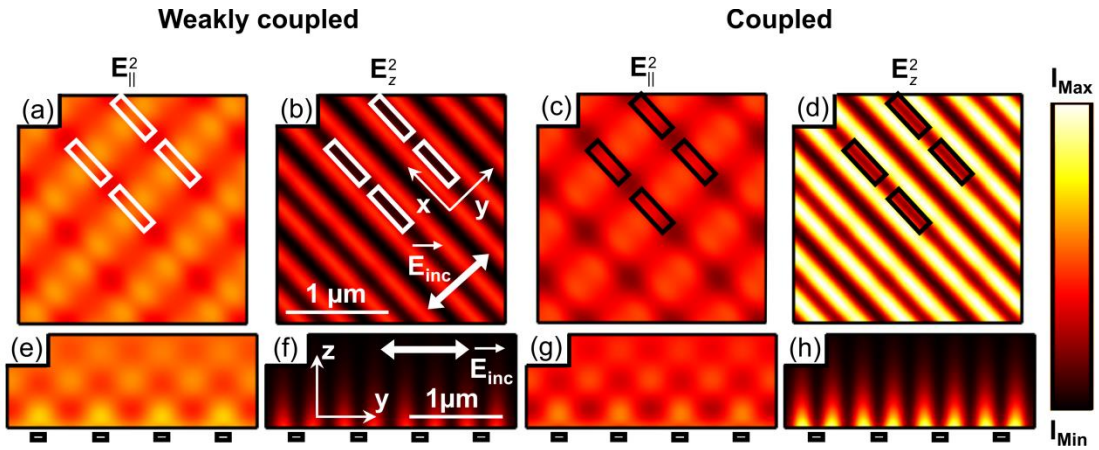

Figure 5. Simulated distributions of the intensity of the in-plane and vertical components of the electric field, $E_{||}^2$ and E_z^2, for the arrays "weakly coupled" and "coupled": (a)-(d) Planar view distributions; (e)-(h) cross-section distributions. The color bar at the side of the images indicate the value of the intensity of $E_{||}^2$ and E_z^2: (a)-(d) $I_{min} = 0.2$; $I_{max} = 2.2$; (e)-(h) $I_{min} = 0$; $I_{max} = 2.2$. Black and white rectangles below or inside the field maps indicate the nanorods position.

Finally, there is still a significant discrepancy between SNOM experiments and simulations when one analyzes in detail the results shown in Figure 3 and 4 for the "coupled" and "coupled close to λ_{SNOM}" situations. In the simulations, the intensity and the degree of vertical delocalization for the "coupled close to λ_{SNOM}" array are much higher than those for the "coupled" one, whereas in the experiments the difference is much smaller. In particular, the vertical scans shown in Figures 4c and d are very similar while Figures 4g and e are clearly distinct. As the field intensity and the degree of vertical delocalization are related to the strength of the geometric resonance, we can associate these differences with the fact that experimentally we illuminate a finite part of the arrays while the simulations take into account infinite arrays. In fact, far-field studies concerning the orthogonal configuration have already established that the

strength of the geometric resonances is affected by the number of periods composing the arrays.[38,39]

We have estimated that the laser spot illuminates about 12 periods of the array in the previously shown SNOM measurements. To further study the influence of the finite size of the illuminated zone on the near–field response, we present in Figure 6 two vertical SNOM images of the "coupled close to λ_{SNOM}" array obtained by highly focusing and defocusing the laser spot. Please note here that, due to experimental limitations, the detected SNOM intensity for the images shown in Figure 6a and c could not be normalized. As a consequence, the obtained intensity values are not comparable since the illumination conditions vary from one SNOM image to the other. The experimental results are compared with the calculated vertical cross-section of E_{tot}^2 for two arrays with 8 and 16 periods. Both simulations and measurements show that the chessboard pattern loses definition with the increase of the number of periods, and that the vertical field delocalization increases as the vertical rising tails (signature of E_z) become more evident, which confirms the influence of the number of involved structures on the strength of the LSPR-$RA_{\|}$ coupling.

In conclusion, we have studied, experimental and numerically, the presence of geometric resonances in arrays of gold nanorods on a glass/air interface. Both the far- and near-field properties of the found resonances have been analyzed. These resonances are generated by the hybridization of the nanostructures LSPR with diffraction orders in the direction of the incident polarization, so that we denote them as parallel collective resonances. This is in clear contrast with the situation usually found in the literature, the orthogonal configuration, where the involved diffraction order is linked to the periodicity perpendicular to the direction of the incident polarization. Further investigation will be needed to understand the physical origin of

this parallel coupling, as the far-field dipolar emission invoked in the orthogonal case is completely out of direction in this configuration. Moreover, the conditions in which parallel and/or orthogonal collective resonances take place need to be identified. We would like to point out here that the parallel resonances are not exclusive of 2D arrays, they can also be sustained by 1D gratings, and they have been previously detected in systems such as gratings of nanowires.[8]

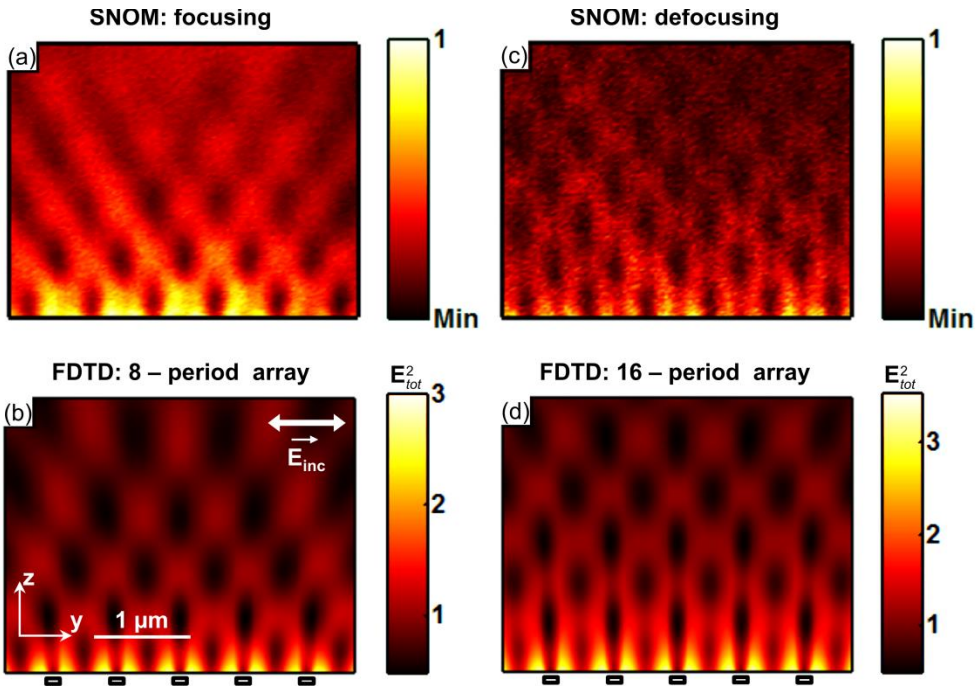

Figure 6. (a) and (c) Vertical SNOM scans, taken with the laser beam tightly focused and defocused, respectively, for the "coupled close to λ_{SNOM}" array. (b) and (d) Cross-section maps of E_{tot}^2 calculated for finite size arrays of 8 and 16 periods, respectively. The color bars next to the simulations indicate the value of E_{tot}^2.

We have demonstrated in the near-field experiments that these parallel collective resonances show a strong vertical field delocalization, which could have interesting applications for sensing or emission enhancement. Indeed, the application of parallel collective resonances for emission enhancement in LED structures has been recently demonstrated.[33] Additionally, our simulations have shown that the electric component normal to the surface, E_z, is the one contributing to the delocalization of the field (this role is attributed to $E_{||}$ in the orthogonal configuration). This

introduces an interesting advantage for the use of collective resonances: an array could be designed to support either parallel or orthogonal ones depending on the electric field component which one needs to enhance. Our far- and near-field results suggest that the strength of the coupling LSPR-$RA_{\parallel}$ increases when the $RA_{\parallel}$ gets closer to the LSPR position. Moreover, the presence of a strong refractive index mismatch between substrate and superstrate does not seem to prevent the formation of a well-defined parallel geometric resonance. Considering that we have detected no hint of orthogonal coupling during our far-field characterization, this suggests a difference of robustness to the index mismatch between the two types of coupling. Even if the origin of this difference needs to be clarified, it is likely to constitute an advantage for the use of these parallel lattice resonances in situations where a high index contrast is unavoidable. The intensity of the field and the amplitude of the delocalization also depend on the number of illuminated periods. We could take advantage of this effect and tune in real time the delocalization and the intensity of the field by varying the size of the illumination spot.

ASSOCIATED CONTENT

Supporting Information Available: Samples fabrication description, details on far- and near-field characterization and FDTD simulations, comparisons between different values of $T_{\perp}$, and development of interferences pattern. This material is available free of charge via the Internet at http://pubs.acs.org.

AUTHOR INFORMATION

Corresponding Author

alan.vitrey@imm.cnm.csic.es, maria-ujue.gonzalez@csic.es.

Author Contributions

A.V. performed most of the near- and far-field experiments and the numerical simulations. P.P. and J.M.G.-M. fabricated the samples. P.P. performed SEM and AFM characterizations. L.A. provided support for the SNOM measurements and carried out a part of them. J.M.G.-M. and M.U.G. conceived the work and contributed to the far-field characterization. A.V., L.A., J.M.G.-M. and M.U.G. discussed the results and wrote the paper.

Notes

The authors declare no competing financial interest.

ACKNOWLEDGMENT

We thank A. García Martín for his help with the FDTD simulations. Funding from Spanish MINECO through grants "FUNCOAT" CONSOLIDER CSD2008-00023, "MAPS" MAT2011-29194-C02-01, and from Comunidad de Madrid through grants "NANOBIOMAGNET" S2009/MAT-1726 and "MICROSERES-CM" S2009/TIC-1476. A. V. acknowledges support from Spanish MINECO through FPI grant. L.A. thanks M. Mortier for providing the fluorescent particles used in the near-field optical experiments.

REFERENCES

(1) Maier, S. A. *Plasmonics: Fundamentals and Applications*; Springer: Berlin, 2007.

(2) Rechberger, W.; Hohenau, A.; Leitner, A.; Krenn, J. R.; Lamprecht, B.; Aussenegg, F. R. *Opt. Commun.* **2003**, *220*, 137–141.

(3) Mühlschlegel, P.; Eisler, H.-J.; Martin, O. J. F.; Hecht, B.; Pohl, D. W. *Science* **2005**, *308*, 1607–1609.

(4) Aćimović, S. S.; Kreuzer, M. P.; González, M. U.; Quidant, R. *ACS Nano* **2009**, *3*, 1231–1237.

(5) Verellen, N.; Sonnefraud, Y.; Sobhani, H.; Hao, F.; Moshchalkov, V. V.; Dorpe, P. V.; Nordlander, P.; Maier, S. A. *Nano Lett.* **2009**, *9*, 1663–1667.

(6) Lassiter, J. B.; Sobhani, H.; Fan, J. A.; Kundu, J.; Capasso, F.; Nordlander, P.; Halas, N. J. *Nano Lett.* **2010**, *10*, 3184–3189.

(7) Lamprecht, B.; Schider, G.; Lechner, R. T.; Ditlbacher, H.; Krenn, J. R.; Leitner, A.; Aussenegg, F. R. *Phys. Rev. Lett.* **2000**, *84*, 4721–4724.

(8) Christ, A.; Zentgraf, T.; Kuhl, J.; Tikhodeev, S. G.; Gippius, N. A.; Giessen, H. *Phys. Rev. B* **2004**, *70*, 125113.

(9) Zou, S.; Janel, N.; Schatz, G. C. *J. Chem. Phys.* **2004**, *120*, 10871–10875.

(10) Markel, V. A. *J. Chem. Phys.* **2005**, *122*, 097101.

(11) Zou, S.; Schatz, G. C. *J. Chem. Phys.* **2005**, *122*, 097102.

(12) Hicks, E. M.; Zou, S.; Schatz, G. C.; Spears, K. G.; Van Duyne, R. P.; Gunnarsson, L.; Rindzevicius, T.; Kasemo, B.; Käll, M. *Nano Lett.* **2005**, *5*, 1065–1070.

(13) Laroche, M.; Albaladejo, S.; Gómez-Medina, R.; Sáenz, J. J. *Phys. Rev. B* **2006**, *74*, 245422.

(14) García de Abajo, F. J. *Rev. Mod. Phys.* **2007**, *79*, 1267–1290.

(15) Auguié, B.; Barnes, W. L. *Phys. Rev. Lett.* **2008**, *101*, 143902.

(16) Kravets, V. G.; Schedin, F.; Grigorenko, A. N. *Phys. Rev. Lett.* **2008**, *101*, 087403.

(17) Giannini, V.; Vecchi, G.; Gómez Rivas, J. *Phys. Rev. Lett.* **2010**, *105*, 266801.

(18) Zhou, W.; Odom, T. W. *Nat. Nanotechnol.* **2011**, *6*, 423–427.

(19) Ghenuche, P.; Vincent, G.; Laroche, M.; Bardou, N.; Haïdar, R.; Pelouard, J.-L.; Collin, S. *Phys. Rev. Lett.* **2012**, *109*, 143903.

(20) Francescato, Y.; Giannini, V.; Maier, S. A. *ACS Nano* **2012**, *6*, 1830–1838.

(21) Zou, S.; Schatz, G. C. *Chem. Phys. Lett.* **2005**, *403*, 62–67.

(22) Chu, Y.; Schonbrun, E.; Yang, T.; Crozier, K. B. *Appl. Phys. Lett.* **2008**, *93*, 181108.

(23) Nikitin, A. G.; Kabashin, A. V.; Dallaporta, H. *Opt. Express* **2012**, *20*, 27941–27952.

(24) Adato, R.; Yanik, A. A.; Amsden, J. J.; Kaplan, D. L.; Omenetto, F. G.; Hong, M. K.; Erramilli, S.; Altug, H. *Proc. Natl. Acad. Sci.* **2009**, *106*, 19227–19232.

(25) Kravets, V. G.; Schedin, F.; Kabashin, A. V.; Grigorenko, A. N. *Opt. Lett.* **2010**, *35*, 956–958.

(26) Offermans, P.; Schaafsma, M. C.; Rodriguez, S. R. K.; Zhang, Y.; Crego-Calama, M.; Brongersma, S. H.; Gómez Rivas, J. *ACS Nano* **2011**, *5*, 5151–5157.

(27) Špačková, B.; Homola, J. *Opt. Express* **2013**, *21*, 27490–27502.

(28) Ausman, L. K.; Li, S.; Schatz, G. C. *J. Phys. Chem. C* **2012**, *116*, 17318–17327.

(29) Vecchi, G.; Giannini, V.; Gómez Rivas, J. *Phys. Rev. Lett.* **2009**, *102*, 146807.

(30) Henson, J.; DiMaria, J.; Dimakis, E.; Moustakas, T. D.; Paiella, R. *Opt. Lett.* **2012**, *37*, 79–81.

(31) Rodriguez, S. R. K.; Lozano, G.; Verschuuren, M. A.; Gomes, R.; Lambert, K.; De Geyter, B.; Hassinen, A.; Van Thourhout, D.; Hens, Z.; Gómez Rivas, J. *Appl. Phys. Lett.* **2012**, *100*, 111103.

(32) Ding, B.; Hrelescu, C.; Arnold, N.; Isic, G.; Klar, T. A. *Nano Lett.* **2013**, *13*, 378–386.

(33) Lozano, G.; Louwers, D. J.; Rodríguez, S. R.; Murai, S.; Jansen, O. T.; Verschuuren, M. A.; Gómez Rivas, J. *Light Sci. Appl.* **2013**, *2*, e66.

(34) Väkeväinen, A. I.; Moerland, R. J.; Rekola, H. T.; Eskelinen, A.-P.; Martikainen, J.-P.; Kim, D.-H.; Törmä, P. *Nano Lett.* **2013**, DOI: 10.1021/nl4035219.

(35) Zhou, W.; Dridi, M.; Suh, J. Y.; Kim, C. H.; Co, D. T.; Wasielewski, M. R.; Schatz, G. C.; Odom, T. W. *Nat. Nanotechnol.* **2013**, *8*, 506–511.

(36) Auguié, B.; Bendaña, X. M.; Barnes, W. L.; García de Abajo, F. J. *Phys. Rev. B* **2010**, *82*, 155447.

(37) Nikitin, A. G.; Nguyen, T.; Dallaporta, H. *Appl. Phys. Lett.* **2013**, *102*, 221116.

(38) Zou, S.; Schatz, G. C. *Nanotechnology* **2006**, *17*, 2813–2820.

(39) Rodriguez, S. R. K.; Schaafsma, M. C.; Berrier, A.; Gómez Rivas, J. *Phys. B Condens. Matter* **2012**, *407*, 4081–4085.

(40) Aigouy, L.; Lalanne, P.; Hugonin, J. P.; Julié, G.; Mathet, V.; Mortier, M. *Phys. Rev. Lett.* **2007**, *98*, 153902.

(41) Aigouy, L.; Prieto, P.; Vitrey, A.; Anguita, J.; Cebollada, A.; González, M. U.; García-Martín, A.; Labéguerie-Egéa, J.; Mortier, M. *J. Appl. Phys.* **2011**, *110*, 044308.